OPEN

EXPERIMENTAL

Characterization of a Murine Pressure Ulcer Model to Assess Efficacy of Adipose-derived Stromal Cells

Amy L. Strong, PhD, MPH*
Annie C. Bowles, MS*
Connor P. MacCrimmon, BSE*
Stephen J. Lee, BSE*
Trivia P. Frazier, PhD*
Adam J. Katz, MD†
Barbara Gawronska-Kozak, PhD‡
Bruce A. Bunnell, PhD*§
Jeffrey M. Gimble, MD, PhD*¶‖**

Background: As the world's population lives longer, the number of individuals at risk for pressure ulcers will increase considerably in the coming decades. In developed countries, up to 18% of nursing home residents suffer from pressure ulcers and the resulting hospital costs can account for up to 4% of a nation's health care budget. Although full-thickness surgical skin wounds have been used as a model, preclinical rodent studies have demonstrated that repeated cycles of ischemia and reperfusion created by exposure to magnets most closely mimic the human pressure ulcer condition.

Methods: This study uses in vivo and in vitro quantitative parameters to characterize the temporal kinetics and histology of pressure ulcers in young, female C57BL/6 mice exposed to 2 or 3 ischemia-reperfusion cycles. This pressure ulcer model was validated further in studies examining the efficacy of adipose-derived stromal/stem cell administration.

Results: Optimal results were obtained with the 2-cycle model based on the wound size, histology, and gene expression profile of representative angiogenic and reparative messenger RNAs. When treated with adipose-derived stromal/stem cells, pressure ulcer wounds displayed a dose-dependent and significant acceleration in wound closure rates and improved tissue histology.

Conclusion: These findings document the utility of this simplified preclinical model for the evaluation of novel tissue engineering and medical approaches to treat pressure ulcers in humans. *(Plast Reconstr Surg Glob Open 2015;3:e334; doi: 10.1097/GOX.0000000000000260; Published online 23 March 2015)*

Older Americans are at increased risk for pressure ulcers (PU) associated with immobilization, diabetes, and peripheral vascular disease.[1–3] The severity of PUs ranges from nonblanching erythema (grade 1) or blisters (grade 2) involving the epidermis and dermis to superficial (grade 3) or deep ulcerations (grade 4) encompassing the underlying skeletal muscle.[4] The incidence of PU has been estimated to be 7.9% in assisted living homes and 18% in nursing homes with an economic burden accounting for 1–4% of the hospital budgets in industrialized nations.[3,5–7] Current standard of care relies on surgical debridement, while the use of growth factors, hyperbaric oxygen, and

Received for publication November 13, 2014; accepted November 13, 2014.

DOI: 10.1097/GOX.0000000000000260

*From the *Center for Stem Cell Research and Regenerative Medicine, Tulane University School of Medicine, New Orleans, La.; †Division of Plastic and Reconstructive Surgery, Department of Surgery, University of Florida, Gainesville, Fla.; ‡Institute of Animal Reproduction and Food Research of Polish Academy of Sciences, Olsztyn, Poland; §Department of Pharmacology, Tulane University School of Medicine, New Orleans, La.; ¶LaCell LLC, New Orleans, La.; ‖Department of Medicine, Tulane Health Sciences Center, New Orleans, La.; and **Department of Surgery, Tulane Health Sciences Center, New Orleans, La.*

negative pressure apparatus remain at the investigational stage. As the number of Americans older than 65 years is one of the fastest growing demographics, the development of improved PU treatment regimens is a high health-care priority.

Over the past decade, fat depots have proven to be a reliable and abundant source of adipose-derived stromal/stem cells (ASCs).[8,9] The ASC are characterized based on their multipotent differentiation ability, proliferative potential, and surface immunophenotype.[9] Additionally, ASC secrete multiple growth factors that promote angiogenesis, vascularization, and tissue repair.[10,11] Recently, full-thickness rodent skin wounds have been used as preclinical models to document the utility and value of stromal/stem cells for epidermal and dermal injuries.[12,13] These studies have demonstrated that topical administration of 3-dimensional ASC spheroids can accelerate healing of full-thickness skin wounds in diabetic mice through the localized release of angiogenic and reparative factors.[14,15]

To date, no studies have evaluated the effects of ASC administration in a PU injury model. Ischemic-reperfusion injury has been implicated as a major mechanism underlying PU injuries.[16,17] Studies by Stadler et al[18] developed a simplified, noninvasive approach to investigate PU injuries in mice. Their method sandwiched the dorsal skin of mice between 2 external magnets, and based on histological and morphological analyses, they documented PU development and resolution occurring over a 21-day period.[18] The current study aimed to further characterize the temporal sequence of PU progression after either 2 or 3 days of cyclic ischemia and reperfusion (IR) in young mice based on quantitative pathophysiological parameters. The model was then used to evaluate the dose-dependent effects of ASC injection on PU injury repair and healing.

Disclosure: *Dr. Gimble is the co-owner, co-founder, and Chief Scientific Officer of LaCell LLC. Drs. Katz and Gawronska-Kozak are consultants to LaCell LLC. None of the other authors has any financial disclosures. This study was supported by the National Institute on Aging of the National Institutes of Health under award number R43AG043904, and funds from this grant was used to pay for the Article Processing Charge.*

Supplemental digital content is available for this article. Clickable URL citations appear in the text.

MATERIALS AND METHODS

PU Model

The Tulane University Institutional Animal Care and Use Committee approved all animal studies and procedures. Six- to 12-week-old female C57BL/6 wild-type mice, purchased from Charles River Laboratories (Wilmington, Mass.), were anesthetized using isoflurane in oxygen for no more than 5 minutes, and hair on the dorsum was shaved (**Supplemental Digital Content 1**, which displays a wound-healing model schematic. Dorsal skin of mice was shaved, subjected to IR cycles, and assessed for 20 days for wound healing, ***http://links.lww.com/PRSGO/A83***). Dorsal skin was positioned between 2 circular 12-mm diameter magnets (Catalog number: CD14C; Master Magnetic Inc., Castle Rock, Colo.) for 12 hours and removed for 12 hours for 1 IR cycle. The force generated between the 2 magnets was 0.183N for a 5-mm skin bridge between the 2 magnets. Mice were divided into 2 magnet exposure groups, resulting in 2 wounds per mouse ($n = 9$ per group): 2 IR cycles versus 3 IR cycles. Mice were provided with food and water ad libitum.

Wound Assessment

Wounds were assessed daily with a digital carbon fiber caliper (Thermo Scientific, Franklin, Mass.) positioned at the borders of the wounds to measure the length and width of each wound. Wound size was calculated based on the area of an ellipse: radius of the length × radius of the width × π. To assess the degree of wound reepithelialization, cotton swabs saturated with 3.0% hydrogen peroxide (Sigma, St. Louis, Mo.) were applied directly on wounds. Visible bubbles on or around the wound borders, indicating oxygen production, signified an open wound and was denoted with a score of 1.[19] The percentage of open wounds was determined relative to the number of wounds in the group. Detailed methods for the histological examination and quantitative reverse-transcriptase polymerase chain reaction (qRT-PCR) can be found in supplemental material (**Supplemental Digital Content 2**, which displays detailed methods for the isolation and characterization of ASCs, ***http://links.lww.com/PRSGO/A84***; **Supplemental Digital Content 3**, which displays primer sequences for qRT-PCR analysis, ***http://links.lww.com/PRSGO/A85***).

Isolation and Expansion of GFP$^+$ ASCs

Detailed methods for the isolation, expansion, and characterization of GFP$^+$ ASCs can be found in supplemental material (**Supplemental Digital Content 2**, which displays detailed methods for the iso-

lation and characterization of ASCs, ***http://links.lww.com/PRSGO/A84***; and Fig. 5). Briefly, ASCs were isolated from inguinal white adipose tissue harvested from transgenic C57BL/6-Tg(UBC-GFP)30Scha/J mice. Adipose tissue was digested in phosphate-buffered saline (PBS, HyClone, Logan, Utah) supplemented with collagenase type I and bovine serum albumin. After digestion, tissue was neutralized with complete culture media (CCM) and centrifuged. Pelleted cells were resuspended in CCM and plated in T175 flasks (CellStar; Greiner Bio One, Monroe, N.C.). Adherent ASCs were washed with PBS, and fresh CCM was replaced every 2–3 days until cells achieved 70% confluence.

Delivery of ASCs

Mice ($n = 3$ per group) were divided into 4 groups: PBS, 1.0×10^5 ASCs, 2.5×10^5 ASCs, or 1.0×10^6 ASCs. Cells were resuspended in a total volume of 100 μL of sterile PBS and injected subcutaneously into each wound with a 27 G ½″ needle (Tyco Healthcare Groups LP, Mansfield, Mass.) and 1 mL Luer-Lok tip syringe (BD, Franklin Lakes, N.J.). The injection site was at the periphery of the wound, and the needle was guided to the base of the wounds where the PBS or ASCs were delivered. All injections were performed under anesthesia, and each mouse received a total volume of 200 μL (100 μL per wound). Injection sites were sealed with Vetbond tissue adhesive (3M Animal Care Products, St. Paul, Minn.) as needles were retracted.

Statistical Analysis

Values are presented as mean ± SD or mean ± standard error of the means. Statistical differences between 2 or more groups were determined by analysis of variance, followed by post hoc Tukey's multiple comparison tests. Statistical significance was set at $P < 0.05$. Analysis was performed using Prism 6.0 (Graphpad Software, San Diego, Calif.).

RESULTS

Determining the Number of IR Cycles for Ideal PU Development

To assess the optimal number of IR cycles required for PU formation, where 1 IR cycle is defined as 12 hours of magnet application followed by 12 hours without magnet application, the dorsal skin was placed between 2 magnets for 2 or 3 IR cycles (**Supplemental Digital Content 1**, which displays a wound-healing model schematic. Dorsal skin of mice was shaved, subjected to IR cycles, and assessed for 20 days for wound healing, ***http://links.lww.com/PRSGO/A83***). Digital imaging demonstrated that skin subjected to 3 IR cycles developed more damage but also healed faster compared with skin subjected to 2 IR cycles (Fig. 1). Three IR cycles resulted in scab formation on day 4, denoted by skin lifting around the edge of the wound, whereas 2 IR cycles resulted in scab formation on day 7 (Fig. 1).

Quantification of wound size with digital calipers accurately correlated with qualitative analysis of skin by digital imaging. Skin subjected to 3 IR cycles underwent significant healing 2 days post defect induction (PDI) from 98.5 to 85.5 mm^2 and continued to heal faster than skin subjected to 2 IR cycles. After 5 days PDI, skin subjected to 3 IR cycles was significantly smaller (75.2 mm^2) than skin subjected to 2 IR cycles (92.5 mm^2; $P < 0.01$; Fig. 2). Following 10 days PDI, skin subjected to 2 and 3 IR cycles was 46.3 mm^2 and 24.1 mm^2, respectively (Fig. 2). There was no significant difference in wound size between 2 and 3 IR cycles after 15 days PDI. H_2O_2 testing for reepithelialization showed earlier formation and resolution of open wounds following 3 IR cycles compared with 2 IR cycles (Fig. 2).

Wounds Display Alterations to the Layers of Skin

To assess the underlying skin, wounds collected following 2 or 3 IR cycles after 5, 10, or 20 days PDI were stained with hematoxylin and eosin or Masson's trichrome. Normal skin displayed 5 distinct layers from the outermost epidermis to the dermis, subcutaneous layer, muscle layer, and hypodermis underneath (Fig. 3A). However, wounds created by IR cycles appeared disorganized, with significant fat necrosis and immune cell infiltration 5 and 10 days PDI (Fig. 3B). After 20 days PDI, wounds resolved and skin showed a reduction in inflammation, cell infiltration, and apoptotic cellular debris; however, the subcutaneous layer remained disorganized (Fig. 3B).

The epidermis of normal skin measured 12.5 μm in thickness, whereas magnet application resulted in significant loss of the epidermis on days 5 and 10 and hypertrophy on day 20 PDI. More specifically, the epidermis subjected to 2 IR cycles measured 1.5, 1.1, and 60.5 μm in thickness after 5, 10, and 20 days PDI, respectively, and the epidermis subjected to 3 IR cycles measured 1.8, 1.6, and 47.9 μm in thickness following 5, 10, and 20 days PDI, respectively ($P < 0.05$; Fig. 3C). Although the thickness of the dermis of normal skin was 182.7 μm, no statistically significant difference in the dermal thickness was observed after 5 or 10 days PDI. However, after 20 days PDI, the thickness of the dermis was increased after 2 (359 μm; $P < 0.01$; Fig. 3C) or 3 IR cycles (379.4 μm; $P < 0.01$; Fig. 3C). The thickness of the subcutaneous layer of normal skin (98.9 μm) was significantly

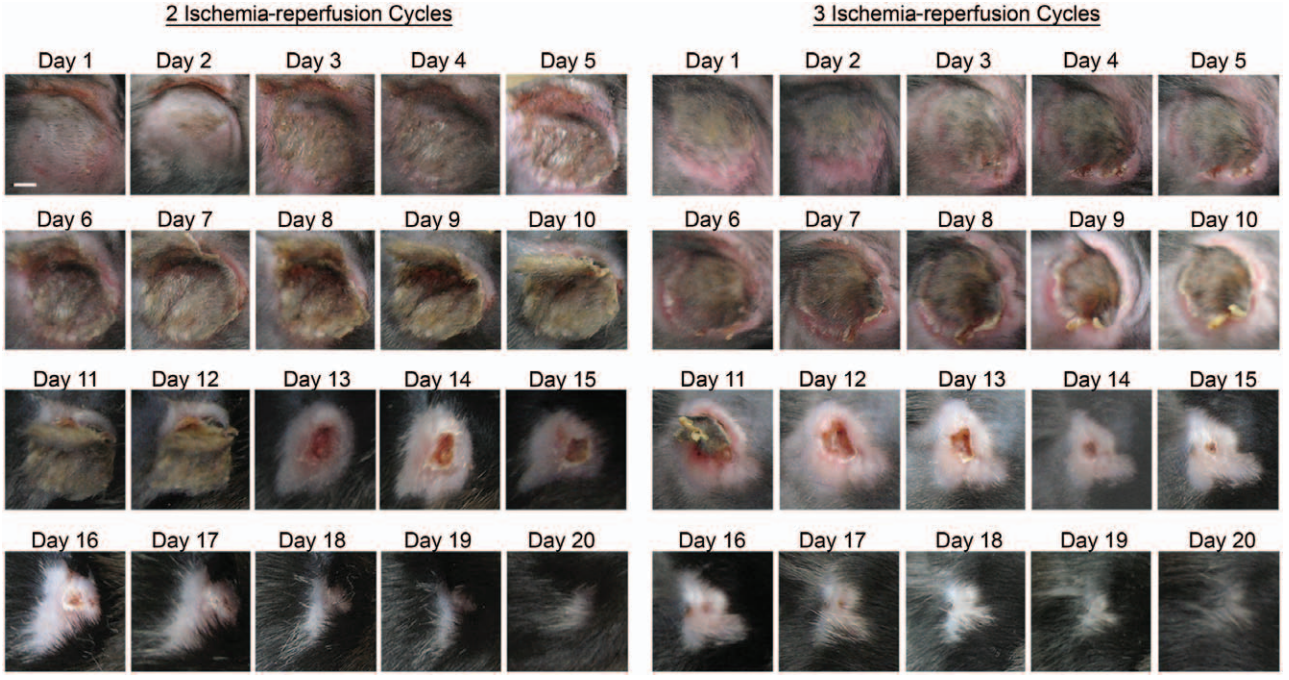

Figure 1. Two IR cycles demonstrate delayed wound healing. Dorsal skin of mice was shaved and subjected to 2 or 3 IR cycles. Digital images were acquired daily, and representative images from the same animal are shown. Scale bar represents 3 mm.

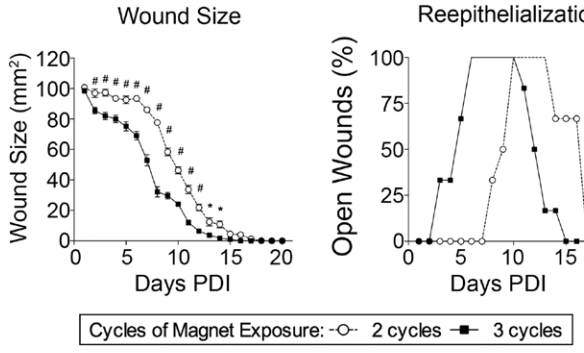

Figure 2. Two IR cycles result in delayed wound closure. Wounds were induced on the dorsal skin of mice by applying 2 or 3 IR cycles. Daily digital caliper measurements of the length and width of the wounds were acquired, and wound size was calculated. Wound closure was determined by soaking cotton swabs in 3% hydrogen peroxide and applied to wounds. The appearance of bubbles was recorded, and the total percentage of wounds open is shown. Mean ± standard error of the mean. *$P < 0.05$; #$P < 0.01$.

thicker than skin induced by 2 (31.0 μm; $P < 0.05$) or 3 IR cycles (42.7 μm; $P < 0.05$) following 20 days PDI. Although the muscle layer was absent after 10 days PDI ($P < 0.01$), it returned to baseline thickness after 20 days PDI, demonstrating the healing potential of young healthy skin.

Tissue exposed to 2 or 3 IR cycles also displayed significantly altered collagen composition (**Supplemental Digital Content 4**, which displays histomorphological analyses of wounds demonstrate remodeling of wounds, ***http://links.lww.com/PRSGO/A86***). Although the collagen in normal skin maintained a basket-weaving appearance, after 5 days PDI, wounds displayed excessive collagen buildup following 2 IR cycles and complete loss of collagen following 3 IR cycles (**Supplemental Digital Content 4**, which displays histomorphological analyses of wounds demonstrate remodeling of wounds, ***http://links.lww.com/PRSGO/A86***). By 20 days PDI, the wounds healed and collagen content increased; however, the collagen lacked organization (**Supplemental Digital Content 4**, which displays histomorphological analyses of wounds demonstrate remodeling of wounds, ***http://links.lww.com/PRSGO/A86***).

Increased Expression of Transforming Growth Factor β, Vascular Endothelial Growth Factor, and Matrix Metalloproteinase 9 and 13 in PUs

To assess molecular changes in key factors involved during wound healing, skin subjected to 2 or 3 IR cycles was collected for RNA extraction and analyzed by qRT-PCR. The expression of transforming growth factor (TGF) β, vascular endothelial growth factor (VEGF), matrix metalloproteinase (MMP) 9, and MMP13 was highest following 5 days PDI. The expression of TGFβ following 5 days PDI by 2 IR cycles and 3 IR cycles was increased 160.6-fold and 35.6-fold, respectively, relative to undamaged skin normalized to 1.0 (Fig. 4). A similar trend was detected in VEGF expression 5, 10, and 20 days PDI induced by 2 IR cycles and 3 IR cycles with 452.7-fold and 11.5-fold in-

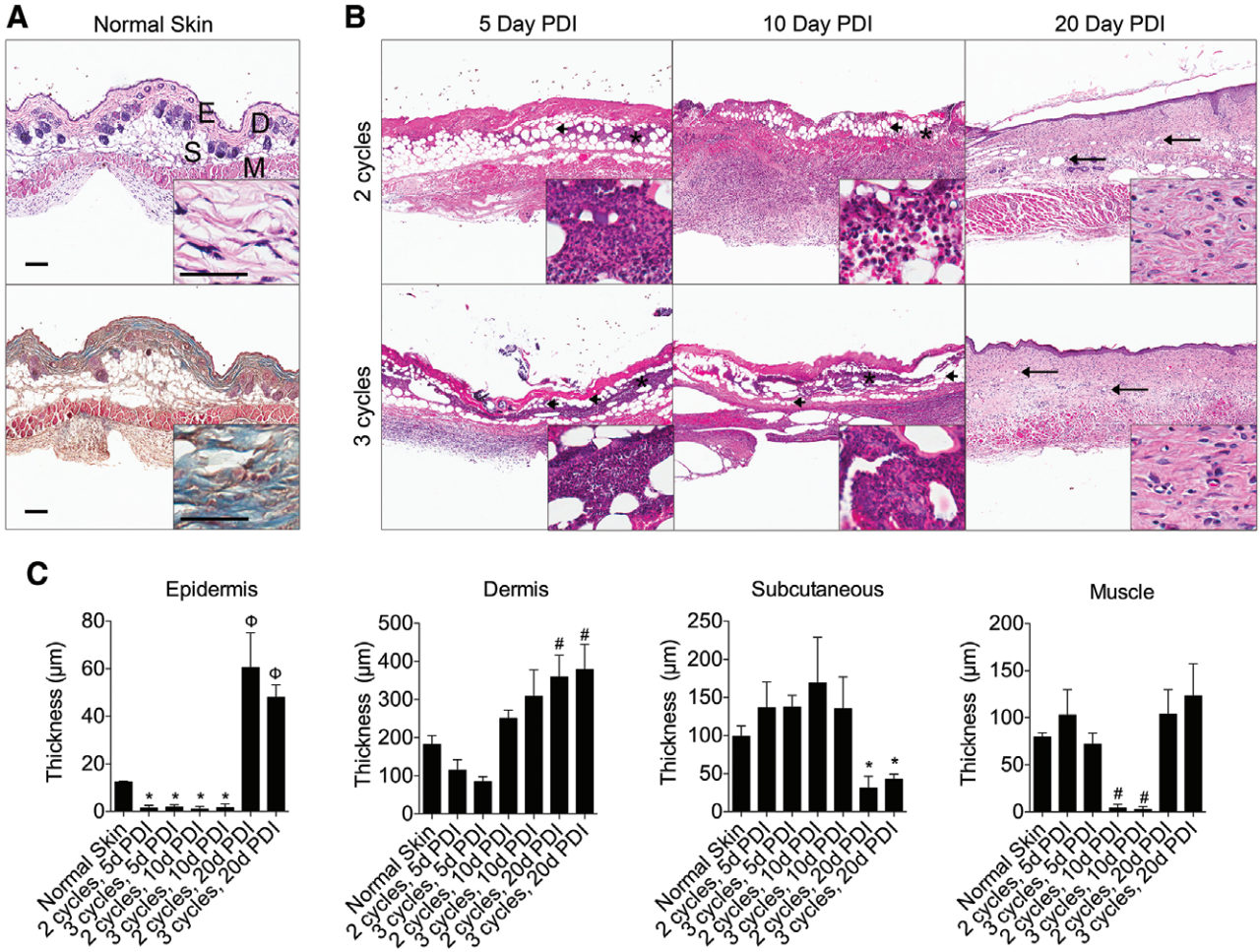

Figure 3. Histomorphological analyses of wounds demonstrate robust inflammatory response and remodeling. Wounds were induced on the dorsal skin of mice with 2 or 3 IR cycles. After 5, 10, or 20 days PDI, mice were killed and wounds were collected, fixed, and stained. A, Representative images of normal skin stained with hematoxylin and eosin (HE) and Masson's trichrome. B, Representative images of skin sections stained with HE showing infiltrating immune cells (asterisk), fat necrosis (arrow head), and disruption of subcutaneous layer (arrow) caused by IR cycles. C, Wounds were induced on the dorsal skin of mice with 2 or 3 IR cycles. After 5, 10, or 20 days PDI, mice were killed and wounds were harvested, fixed, and stained with HE. Thickness of epidermis, dermis, subcutaneous tissue, and muscle is shown (n = 3/time point). Mean ± standard error of the mean. *$P < 0.05$; #$P < 0.01$; Φ$P < 0.001$. D indicates dermis; E, epidermis; M, muscle layer; and S, subcutaneous layer.

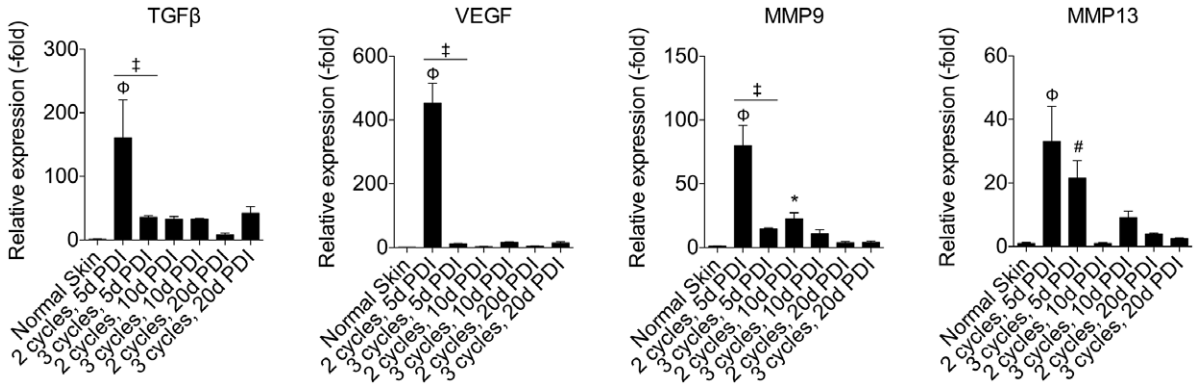

Figure 4. Pressure ulcer wounds display increased expression of TGFβ, VEGF, MMP9, and MMP13. Skin subjected to 2 or 3 IR cycles was harvested 5, 10, or 20 days PDI for RNA extraction, complementary DNA transcription, and qRT-PCR analysis. Data are normalized to normal, healthy age-matched skin, set to 1.0. Mean ± SD. *$P < 0.05$, #$P < 0.01$; Φ$P < 0.001$ relative to normal skin; ‡$P < 0.001$ between 2 IR cycles and 3 IR cycles.

creases, respectively, relative to healthy skin (Fig. 4). MMP9 expression in wounds 5 days PDI after 2 IR cycles and 3 IR cycles was 79.8-fold and 14.6-fold, respectively, relative to healthy skin (Fig. 4). Expression of MMP13 after 5 days PDI of 2 IR cycles and 3 IR cycles increased 33.1-fold and 21.5-fold, respectively, normalized to healthy skin (Fig. 4).

ASCs Accelerate Wound Healing of PUs in a Dose-dependent Manner

ASCs were characterized by morphological appearance, differentiation capacity, cell surface marker profile, and the ability to form colony-forming units (Fig. 5). ASCs displayed a spindle shape-like morphology, fluoresced green, maintained the capacity to form colony-forming units when plated at low density, were able to undergo osteogenic and adipogenic differentiation, and expressed the following cell surface marker profile: $CD29^+$, $CD34^+$, $Sca\text{-}1^+$, $CD11b^-$, $CD31^-$, $CD45^-$ (data not shown, unpublished observation, Lee et al, 2014). Due to the prolonged healing period required for wounds subjected to 2 rather than 3 IR cycles, experiments to monitor ASC acceleration of PU healing were conducted using the 2 IR cycle model.

The 2 IR cycle PU was treated with PBS alone, 1.0×10^5 ASCs, 2.5×10^5 ASCs, or 1.0×10^6 ASCs. Wounds treated with ASCs displayed accelerated wound healing compared with PBS-treated wounds (Fig. 6A). On day 10 PDI, wound sizes were 55.9, 42.7, 43.3, and 22.3 mm^2 following treatment with PBS, 1.0×10^5 ASCs, 2.5×10^5 ASCs, and 1.0×10^6 ASCs, respectively ($P < 0.001$; Fig. 6B). Healing was significantly enhanced in the wounds treated with 1.0×10^6 ASC compared with wounds treated with 1.0×10^5 ASCs or 2.5×10^5 ASCs ($P < 0.001$; Fig. 6B). All wounds were remained open on day 10.

The thickness of the layers of skin treated with ASCs was assessed following 10 days PDI. Treated wounds displayed increased thickness of the epidermis to 91.8, 82.5, 80.6, and 44.9 μm following treatment with PBS, 1.0×10^5 ASCs, 2.5×10^5 ASCs, and 1.0×10^6 ASCs, respectively (Fig. 7). Wounds treated with the highest concentration of ASCs displayed the least epidermal hypertrophy. Likewise, the dermis demonstrated hypertrophy following injection of PBS or cells; however, treatment with ASCs at higher dosages reduced the dermal thickness from 265.2 μm in PBS treated to 231.6 μm (1.0×10^5 ASCs), 164.4 μm (2.5×10^5 ASCs; $P < 0.05$), and 163.2 μm (1.0×10^6 ASCs; $P < 0.05$; Fig. 7). Subcutaneous layers of wounds treated with ASCs also displayed reduced thickness compared with PBS-treated skin. The thickness of the subcutaneous layer of PBS-treated wounds was 156.8 μm, whereas the thickness of the subcutaneous layer of 1.0×10^5 ASCs, 2.5×10^5 ASCs, and 1.0×10^6 ASCs was 107.6, 55.8, and 87.2 μm, respectively (Fig. 7). With respect to the muscle, ASCs restored the muscular layer of skin following 10 days PDI. PBS-treated wounds did not have a muscular layer, whereas ASC-treated wounds restored the muscular layer to 75.6, 42.3, and 126.2 μm with 1.0×10^5 ASCs, 2.5×10^5 ASCs, and 1.0×10^6 ASCs, respectively. These results suggest that ASC treatment accelerates wound healing, restoring the cellular architecture of the damaged/injured skin.

DISCUSSION

Temporal Kinetics and Quantitative Parameters of the PU Model

With the aging demographic of the world's population, a greater number of individuals will be at

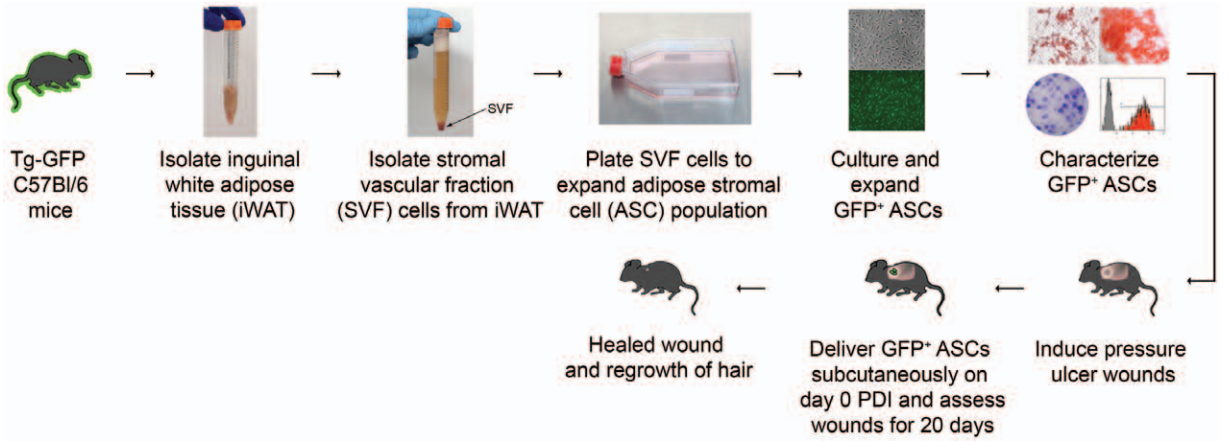

Figure 5. Schematic of ASC delivery in PU model. Inguinal white adipose tissue was isolated from transgenic GFP^+ C57Bl/6 mice, digested with collagenase to harvest SVF cells, and plated in a T175 plate for expansion. Cells were characterized prior to injection into mice exposed to 2 IR cycles, and wounds were assessed for 20 days for wound healing. *Repeated 2 additional times for a total of 3 IR cycles.

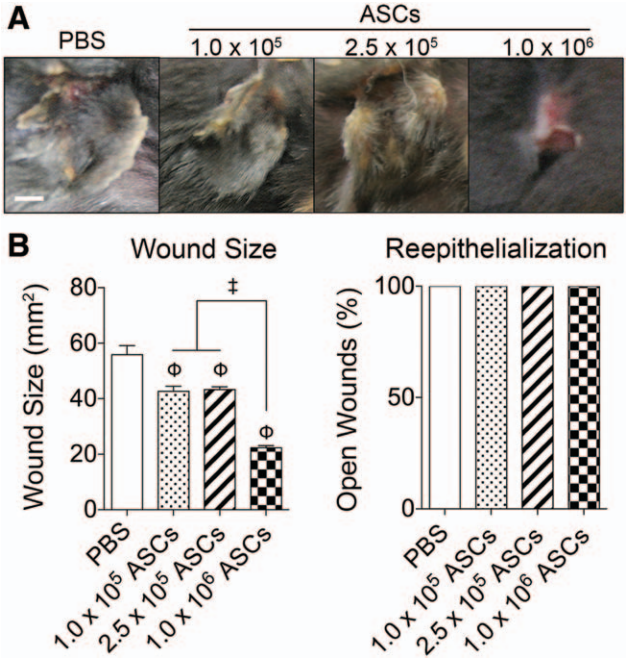

Figure 6. ASC treatment accelerates wound healing in a dose-dependent manner. Dorsal skin of mice was subjected to 2 IR cycles and treated with PBS, 1.0×10^5 ASCs, 2.5×10^5 ASCs, or 1.0×10^6 ASCs. A, Representative images of wounds 10 days after treatment are shown. B, Wound size and percentage of wounds open 10 days after treatment are shown. Mean ± standard error of the mean. Φ$P < 0.001$ relative to PBS-treated wounds; ‡$P < 0.001$ relative to 1.0×10^6 ASC-treated wounds. Scale bar represents 3 mm.

risk for the development of PU injuries in the next decade. Consequently, there is a need for a defined and reproducible animal model of PU. Although a full-thickness surgical skin wound has been an important experimental model, the IR injury created in rodents by cycles of magnetic application best mimics the PU injury in human patients. The current study has used quantitative parameters to refine and simplify the IR cycle number in the murine PU model, documenting the reproducible induction of injury with 2 IR cycles rather than 3 IR cycles as originally described.[18] This revised PU model has been used to test and document the feasibility and utility of ASC injection as a medical therapeutic.

Morphologically, the current study demonstrated a time-dependent development and healing of the skin lesion following IR injury over a 20-day period. Wound sizes were consistent with the temporal kinetics described by Saito et al.[20] It was noteworthy that the recovering injury site was initially covered with white hair and that melanin pigmentation returned only after the complete closure of the wound. This suggests that further studies should be conducted to evaluate the recovery of melanocytes in the PU model. The tissue architecture after both 2 IR cycles and 3 IR cycles was comparable and consistent with the original findings reported by Peirce et al[21] and Stadler et al.[18] The difference observed in wound-healing rates between the 2 IR cycles and 3 IR cycles could reflect the development of full necrosis sooner in the 3 IR cycle, resulting in earlier clearing of the necrosis tissue and healing. Furthermore, the differences in epithelial thickness between the 2 IR cycles and 3 IR cycles could reflect temporal differences along the wound-healing continuum. Detailed kinetic analyses by Saito et al[20] documented the rapid infiltration of leukocytes and macrophages within 3 days following the PU injury.

At the molecular level, the current study documented the temporal kinetics of representative angiogenic (*VEGF*) and reparative (*TGF*β, *MMP9*, *MMP13*) messenger RNAs (mRNAs) following the PU formation. All biomarkers were elevated relative to control tissue with maximal levels at 5 days PDI. These findings are consistent with those of Saito et al,[20] who documented increased mRNA levels of the inflammatory cytokines and biomarkers interleukin-1 beta, interleukin-6, inducible nitric oxide synthase, and monocyte chemoattractant protein 1 within 3 days PDI. As the mRNA increases in the current study were greater with 2 IR cycles rather than 3 IR cycles, it is possible that investigating earlier temporal kinetics with 3 IR cycles would reveal higher expression of these genes at earlier time points. Furthermore, the increased levels of cytokines in the 2 IR cycles would also suggest that not only there were a significant number of injured cells at day 5 but also the viable cells capable of cytokine and growth factor secretion persisted within the wound bed. Overall, the maximal induction of the mRNAs seems to coincide with the onset of tissue repair and inflammatory cell infiltration as opposed to later events.

PU Model Assessment of ASC Healing Efficacy

The medical utility of the simplified IR-induced PU model was validated by testing ASC efficacy in a dose-dependent manner. The injection of murine ASCs into the PU wound significantly accelerated wound closure relative to vehicle (PBS)-treated controls. Additionally, histology in the ASC cohorts displayed reduced levels of epidermal and dermal hypertrophy and improved recovery of subcutaneous adipose and muscle morphology. Maximal efficacy was obtained with injection of 10^6 ASC per wound in 2- to 3-month-old mice. Prior studies using a surgical full-thickness skin wound model compared the response of young control and diabetic mice to topical treatment with ASC spheroids. Although ASC treatment accelerated wound closure rates in the diabetic cohort, it did not improve the recovery rate in the controls.[14] In con-

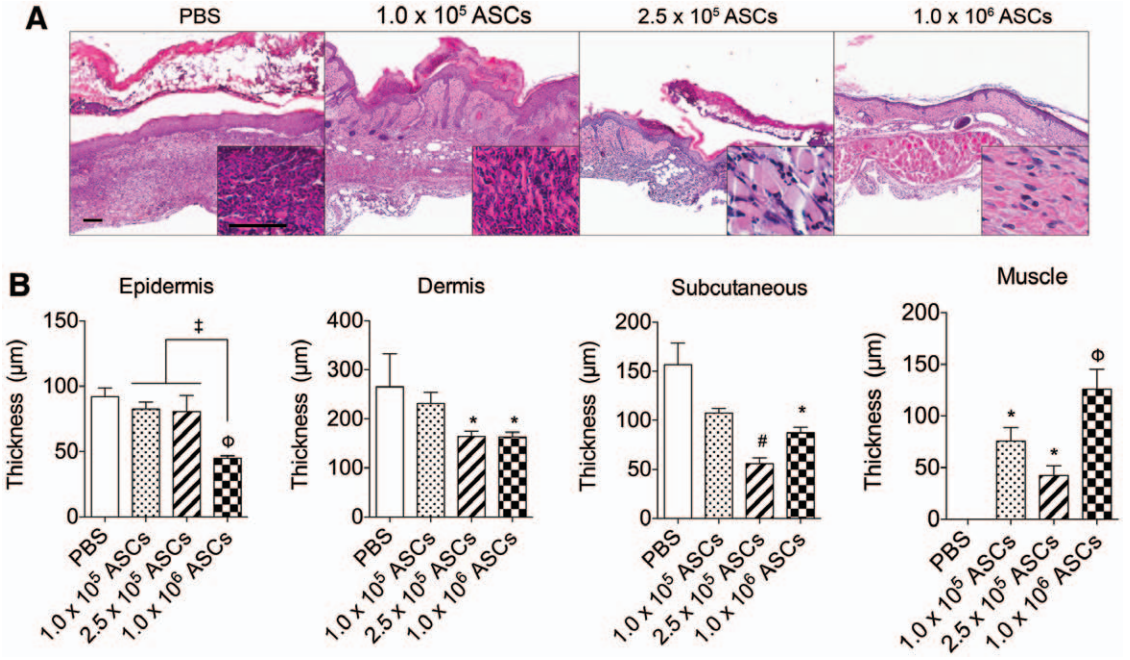

Figure 7. ASCs restore normal skin architecture by reducing hypertrophy. Dorsal skin of mice was subjected to 2 IR cycles and treated with PBS, 1.0×10^5 ASCs, 2.5×10^5 ASCs, or 1.0×10^6 ASCs. A, Representative images of skin sections stained with hematoxylin and eosin (HE) showing reduced infiltrating immune cells following PBS or ASC treatment. Scale bar represents 50 μm. B, After 10 days post defect induction, mice were killed and wounds were harvested, fixed in formalin, and stained with HE. Thickness of epidermis, dermis, subcutaneous tissue, and muscle is shown (n = 3/time point). *P < 0.05; #P < 0.01; ΦP < 0.001 relative to PBS-treated wounds; ‡P < 0.001 relative to 1.0×10^6 ASC-treated wounds.

trast, the current study demonstrates that ASC therapy can significantly improve epidermal and dermal recovery in young mice in the absence of any underlying disease. This difference in outcomes may reflect the mode of ASC delivery and suggests that subcutaneous injection, as opposed to topical delivery, is advantageous. Other explanations include the use of other murine strains, the utilization of alternative wound induction methods, and the underlying pathophysiology of diabetes as opposed to IR injury.

Independent studies have demonstrated that growth factors, such as basic fibroblast growth factor or erythropoietin; biomaterials, such as glycosaminoglycans; and increased subcutaneous adiposity prevent injury and/or improve recovery of IR injuries caused by magnet application.[22–25] Although future studies will be necessary to determine if these contribute to the ASC effect, the current study provides proof of principle evidence that ASCs improve PU injury recovery in a dose-dependent manner. Furthermore, these findings validate the utility of the simplified PU model for the evaluation of novel tissue engineering and medical therapeutics. As a next step, the model will be used to compare the impact of ASC therapy on PU recovery between young (2–4 months old) and old (24–26 months old) mice. It is anticipated that the outcomes from these preclinical studies will provide the basis for clinical translation of ASC therapies to treat PU injuries in patients. Additionally, the PU model can be used to evaluate the effects of alternative therapies, such as biocompatible scaffolds or cytokine/protein-based interventions.

Jeffrey M. Gimble, MD, PhD,
1441 Canal Street, Suite 304,
New Orleans, LA 70112.
E-mail: jeffrey.gimble@lacell-usa.com

ACKNOWLEDGMENTS

We thank Dina Gaupp, H. Alan Tucker, Forum Shah, and Xiying Wu for their technical expertise. We also thank Dr. Donald P. Gaver in the Department of Biomedical Engineering at Tulane University for his engineering expertise.

REFERENCES

1. Clemens MW, Broyles JM, Le PN, et al. Innovation and management of diabetic foot wounds. *Surg Technol Int.* 2010;20:61–71.
2. Vangilder C, Macfarlane GD, Meyer S. Results of nine international pressure ulcer prevalence surveys: 1989 to 2005. *Ostomy Wound Manage.* 2008;54:40–54.
3. White-Chu EF, Flock P, Struck B, et al. Pressure ulcers in long-term care. *Clin Geriatr Med.* 2011;27:241–258.
4. Stausberg J, Kiefer E. Classification of pressure ulcers: a systematic literature review. *Stud Health Technol Inform.* 2009;146:511–515.

5. Trueman P, Whitehead SJ. The economics of pressure relieving surfaces: an illustrative case study of the impact of high-specification surfaces on hospital finances. *Int Wound J.* 2010;7:48–54.
6. Makai P, Koopmanschap M, Bal R, et al. Cost-effectiveness of a pressure ulcer quality collaborative. *Cost Eff Resour Alloc.* 2010;8:11.
7. Flack S, Apelqvist J, Keith M, et al. An economic evaluation of VAC therapy compared with wound dressings in the treatment of diabetic foot ulcers. *J Wound Care* 2008;17:71–78.
8. Gimble JM, Katz AJ, Bunnell BA. Adipose-derived stem cells for regenerative medicine. *Circ Res.* 2007;100:1249–1260.
9. Bourin P, Bunnell BA, Casteilla L, et al. Stromal cells from the adipose tissue-derived stromal vascular fraction and culture expanded adipose tissue-derived stromal/stem cells: a joint statement of the International Federation for Adipose Therapeutics and Science (IFATS) and the International Society for Cellular Therapy (ISCT). *Cryotherapy* 2013;15:641–648.
10. Kilroy GE, Foster SJ, Wu X, et al. Cytokine profile of human adipose-derived stem cells: expression of angiogenic, hematopoietic, and pro-inflammatory factors. *J Cell Physiol.* 2007;212:702–709.
11. Kapur SK, Katz AJ. Review of the adipose derived stem cell secretome. *Biochimie* 2013;95:2222–2228.
12. Altman AM, Yan Y, Matthias N, et al. IFATS collection: human adipose-derived stem cells seeded on a silk fibroin-chitosan scaffold enhance wound repair in a murine soft tissue injury model. *Stem Cells* 2009;27:250–258.
13. Schatteman GC, Ma N. Old bone marrow cells inhibit skin wound vascularization. *Stem Cells* 2006;24:717–721.
14. Amos PJ, Kapur SK, Stapor PC, et al. Human adipose-derived stromal cells accelerate diabetic wound healing: impact of cell formulation and delivery. *Tissue Eng Part A* 2010;16:1595–1606.
15. Nie C, Yang D, Xu J, et al. Locally administered adipose-derived stem cells accelerate wound healing through differentiation and vasculogenesis. *Cell Transplant.* 2011;20:205–216.
16. Kosiak M. Etiology and pathology of ischemic ulcers. *Arch Phys Med Rehabil.* 1959;40:62–69.
17. Daniel RK, Priest DL, Wheatley DC. Etiologic factors in pressure sores: an experimental model. *Arch Phys Med Rehabil.* 1981;62:492–498.
18. Stadler I, Zhang RY, Oskoui P, et al. Development of a simple, noninvasive, clinically relevant model of pressure ulcers in the mouse. *J Invest Surg.* 2004;17:221–227.
19. AlDahlawi S, Eslami A, Häkkinen L, et al. The alphav-beta6 integrin plays a role in compromised epidermal wound healing. *Wound Repair Regen.* 2006;14:289–297.
20. Saito Y, Hasegawa M, Fujimoto M, et al. The loss of MCP-1 attenuates cutaneous ischemia-reperfusion injury in a mouse model of pressure ulcer. *J Invest Dermatol.* 2008;128:1838–1851.
21. Peirce SM, Skalak TC, Rodeheaver GT. Ischemia-reperfusion injury in chronic pressure ulcer formation: a skin model in the rat. *Wound Repair Regen.* 2000;8:68–76.
22. Demiot C, Sarrazy V, Javellaud J, et al. Erythropoietin restores C-fiber function and prevents pressure ulcer formation in diabetic mice. *J Invest Dermatol.* 2011;131:2316–2322.
23. Nguyen-Tu MS, Begey AL, Decorps J, et al. Skin microvascular response to pressure load in obese mice. *Microvasc Res.* 2013;90:138–143.
24. Park CJ, Clark SG, Lichtensteiger CA, et al. Accelerated wound closure of pressure ulcers in aged mice by chitosan scaffolds with and without bFGF. *Acta Biomater.* 2009;5:1926–1936.
25. Wassermann E, van Griensven M, Gstaltner K, et al. A chronic pressure ulcer model in the nude mouse. *Wound Repair Regen.* 2009;17:480–484.